Skin Formation and Water Distribution in Semicrystalline Polymer Layers Cast from Solution: A Magnetic Resonance Imaging Study

Elisabetta Ciampi and Peter J. McDonald*

School of Electronics and Physical Sciences, Department of Physics, University of Surrey, Guildford, Surrey GU2 7XH, UK

Received July 7, 2003; Revised Manuscript Received August 27, 2003

ABSTRACT: Magnetic resonance imaging (MRI) using FLASH and GARField is used to measure the water distribution as a function of time in layers of poly(vinyl alcohol) (PVOH) cast from aqueous solution. It is shown that the water distribution remains uniform in thin layers dried slowly but is nonuniform in thicker layers dried more quickly. Moreover, it is shown that layers dried slowly in comparison to a time characteristic of the amorphous−crystalline transition develop a crystalline skin whereas other layers do not. These results are described in terms of a parameter space defined by a (dimensionless) Peclet number for the layer and a dimensionless drying time. The magnetic resonance imaging results and interpretation are supported by pulsed field gradient measurements of polymer and water diffusion coefficients and also by differential scanning calorimetry (DSC) measurements of dried layers.

1. Introduction

Glassy polymer films have widespread uses, for instance as coating materials. A common means to achieve a glassy layer is to coat the substrate in a viscous solution of the polymer and allow it to dry. This basic industrial process has attracted interest of late in part due to increasing environmental concerns. There is a need to reduce both the energy input into the drying process and the use of volatile organic compounds. Advance is hampered by a lack of real understanding of the drying process itself. In the case of polymers that are glassy at room temperature, the polymer first becomes rubbery as solvent is removed by evaporation. With further drying, the solvent-induced glass transition at the drying temperature is passed, and the polymer becomes glassy. Specific questions concern the formation of a glassy skin on the layer which can significantly inhibit solvent loss so slowing the process and which at worst can trap residual solvent in the lowest layers of the polymer. In the case of semicrystalline polymers there is the additional complication that the glassy polymer can develop both amorphous and crystalline regions. Not only does crystallinity affect the properties of the final layer, but it can also affect the drying process as the crystalline regions tend to be less permeable than the amorphous regions.

There have been a number of both theoretical and experimental studies looking at the drying of solutions of glassy polymers. For instance, Romdhane et al.[1] investigated the drying of poly(methyl methacrylate) films cast from toluene by gravimetric and thermal analysis and compared the experimental results with a detailed Fickian diffusion-based model of drying in which various forms of the diffusivity were compared. Ngui and Mallapragada[2−4] studied the drying of semicrystalline poly(vinyl alcohol) (PVOH) using a combination of techniques including thermogravimetric analysis, differential scanning calorimetry, and Fourier transform infrared spectroscopy. They compared their data to an alternate diffusion-based model which additionally included the development of crystalline regions. Vinjamur and Cairncross[5] described how a skin can trap residual solvent behind it and presented a diffusion model to describe the effect. Their model is non-Fickian since it includes a term to describe stresses in the polymer. Finally, Hoshida and Miyashita[6] investigated the drying of layers of poly(vinyl acetate) solution containing both toluene and ethylbenzene by thermogravimetric analysis and interpreted their results in terms of yet another diffusion-based model. While these previous studies all met with some success in understanding the drying of polymer solutions, a common limitation is a lack of spatially resolved information about the composition profile of drying layers. It is the purpose of our study to overcome this limitation.

In our study, we use magnetic resonance profiling to follow noninvasively the spatial and temporal dependence of the water concentration in drying layers of PVOH solution from a few hundred microns to a couple of millimeters thick. To the best of our knowledge, this is the first time that drying PVOH layers have been examined in this way. This contrasts with the considerable body of literature examining the use of magnetic resonance imaging to asses liquid ingress into, and dissolution of, polymers including PVOH.[7] The work reported here uses a novel magnet design known as GARField,[8] standing for gradient at right angle to field, and extends our ongoing studies of the drying of aqueous dispersion coating systems. Magnetic resonance profiling probes the resonant frequency of ^{1}H nuclei in a magnetic field gradient to yield a one-dimensional map. The signal intensity is weighted both by the local ^{1}H concentration and by molecular mobility. The latter provides a valuable contrast mechanism between, for instance, mobile water in solution and polymer. Using the GARField magnet, it is possible to obtain spatial resolution of the order of 10 μm and temporal resolution of the order of 1 min from drying layers. Previous studies with GARField have looked at the drying of cross-linking latex dispersions,[9] alkyd emulsions,[10,11] and wood-glue layers.[12] In the case of alkyd emulsions in particular, the effects of skinning have been made apparent, and some of the ideas adopted in this study

* Author to whom correspondence should be addressed.

10.1021/ma034951j CCC: $25.00
Published on Web 10/07/2003

stem from this work. The measurements made with GARField are supported by conventional magnetic resonance microscopy measurements[13] of drying PVOH layers, pulsed-field-gradient magnetic resonance[13] and fringe field diffusometry measurements[14] of water and polymer self-diffusion coefficients, respectively, in polymer solutions, and by differential scanning calorimetry of the dried polymer layers.

In principle, it is possible to fit the concentration profiles obtained using GARField to detailed, diffusion-based models of drying such as those already discussed. The difficulty in doing this is to know accurately the large number of model parameters required and in particular the concentration dependence of the diffusivity. We therefore prefer to adopt an alternate, semiquantitative analysis which has the merit of enabling a reasonable prediction of the principal features of the drying layer. This analysis comes in part from ideas first proposed by Routh and Russel.[15] These authors proposed that an initial Peclet number characteristic of the layer can be used to predict the circumstances under which skinning of a drying dispersion layer might be expected. The Peclet number balances the effects of particle diffusion in the film, which tends to maintain a uniform particle concentration across the depth of the film, against the effects of evaporation, which tends to concentrate particles near the surface. A large Peclet number leads to a prediction of nonuniform drying and a small one to uniform drying. The Peclet number proposed by Routh and Russel is merely a characteristic parameter for the dispersion at the outset of drying. Here we attempt to evaluate the Peclet number for the polymer solution *throughout* the process under the worst case scenario of constant free evaporation. We also compare the drying time to a characteristic time for the formation of crystallites and examine how this affects the drying profile. The Peclet number and the ratio of the drying time to the time required for crystallite formation define a two-dimensional parameter space across which different drying behaviors are expected and observed. We present examples of layers typical of different regions in this space. This simplified analysis offers a ready means to predictive description of likely drying behavior.

2. Theory

While models such as those due to Ngui and Mallapraga,[3] Vinjamur and Cairncross,[5] and other authors have considerable merit, a significant practical difficulty in their application is the very large number of parameters which are required in order to quantitatively analyze experimental concentration profile data. For this reason we prefer to interpret our data in terms of a much simpler model following in part ideas proposed by Routh and Russel[15] for the analysis of drying dispersions.

2.1. Peclet Analysis. In heat transfer problems, a Peclet, *Pe*, number balances bulk to conductive heat transfer. Elsewhere, it balances hydrodynamic forces to Brownian motion. A number akin to a Peclet number is defined here to characterize the relative strength of evaporative drying, which tends to lead to surface concentration of the polymer solution, and polymer diffusion in the solution, which tends to equilibrate the layer spatially. Hence

$$Pe = \frac{HE}{D} \tag{1}$$

where H is the layer thickness, E is the evaporation rate, and D is the diffusion coefficient for the water/polymer solution. When $Pe \gg 1$, the evaporation is too fast and the layer too thick for interdiffusion of the water and polymer chains to maintain a uniform polymer concentration. Nonuniform drying is expected. The surface layer is more concentrated and eventually turns glassy before the lower bulk. Conversely, when $Pe \ll 1$, the situation is reversed, and the polymer concentration in the layer remains uniform. In Routh and Russell's initial theoretical analysis of dispersions, and our own verification of it using MR, the initial (time zero) value of *Pe* was used to characterize the layer. This met with some success. However, both the diffusion coefficient and thickness change with time throughout the drying. Consequently, we now estimate the *Pe* number continuously throughout the drying process. The implicit assumption is made that, before nonuniformity develops, the layer is of uniform concentration and therefore characterized throughout its depth by a single diffusion coefficient and polymer fraction.

The required diffusivity is the mutual diffusion coefficient for PVOH/water as a function of concentration. However, we can more easily measure self-diffusion using pulsed-field-gradient NMR. Following de Gennes,[16] we write that the self-diffusivity of the water in the solution, D_{SW}, is

$$D_{SW}(\phi) = D_0 \exp\left(-\frac{a}{1-\phi}\right) \tag{2}$$

where D_0 and a are constants, the latter of the order of unity, and ϕ is the polymer fraction. The polymer fraction is a function of time t and is given by

$$\phi(t) = \frac{H_0}{H(t)}\phi_0 \tag{3}$$

where H_0 is the initial layer thickness and ϕ_0 is the initial polymer fraction. Under the worst case scenario of constant evaporation equal to the initial rate which is most likely to lead to spatially nonuniform drying

$$H(t) = H_0 - Et \tag{4}$$

The link between solvent and polymer self-diffusivities and the polymer−solvent mutual diffusion coefficient as a function of concentration is notoriously complex. It has been studied theoretically by several authors,[17−19] but there remains a paucity of experimental data by which any of the analyses can be rigorously tested. However, most models[20−24] show a mutual diffusivity which increases rapidly as water is added to the dry polymer before reaching a broad maximum at a high water content and then decreasing again. The exceptions to this general picture have the diffusivity increasing across the whole water concentration range.[25] The existence of the broad maximum is perhaps counterintuitive but is attributed to polymer chain interactions. We choose to follow the model proposed by Alsoy and Duda,[26] which offers a reasonable compromise between simplicity of final result and degree of analytical rigor. These authors suggest

$$D = D_{SW}\phi(1 - 2\chi + 2\chi\phi) \tag{5}$$

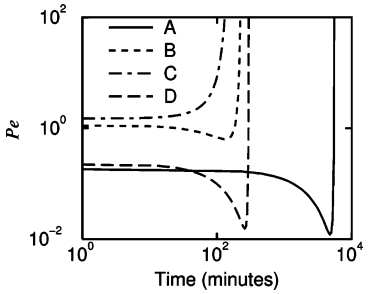

Figure 1. Time dependence of the Peclet number, *Pe*, for the four drying layers described in the text.

where χ is the Flory−Huggins interaction parameter for water and PVOH. As a first approximation, χ can be estimated from the second osmotic virial coefficient A_2[27] using

$$\chi = 0.5 - \rho_P^2 V_W A_2 \tag{6}$$

where ρ_P is the density of the polymer (1.29 g/cm^3),[28] V_W is the molar volume of water, and A_2 is (3.9−5.2) × 10^{-4} mol cm^3/g^2.[28] This gives $\chi = 0.49$.

Strictly, the theory of Alsoy and Duda is valid only below ϕ_g, where ϕ_g is the polymer fraction at the solvent-induced glass transition. This critical concentration can be calculated from the Fox−Flory equation

$$\frac{1}{T_g} = \frac{\phi_g}{T_g^p} + \frac{1-\phi_g}{T_g^w} \tag{7}$$

where T_g is the glass transition temperature of the mixture, and T_g^p and T_g^w are the glass transition temperatures of pure PVOH (85 °C)[28] and pure water (−135 °C),[29] respectively. At room temperature, ϕ_g is approximately equal to 0.87. In practice, extrapolating eq 5 beyond ϕ_g, rather than using a more complete analysis, does not substantially affect our results or conclusions.

Figure 1. shows plots of *Pe* evaluated using eqs 2−5, as a function of *t*, for four different initial parameter sets equating to the conditions of the experiments reported below. It is immediately evident that *Pe* gently decreases during the major part of drying—that is, the diminishing layer thickness wins over the varying diffusivity—and that it only substantially increases in the very late stages. Only for layer C, which has a very high initial polymer fraction, is this not true. In this case reducing diffusivity wins from the outset.

2.2. Crystallinity. In cases of nonuniform drying where a concentrated surface layer develops, it is important to ask whether the surface is substantially amorphous or crystalline. In semicrystalline polymers the crystalline content of the polymer has a profound effect on the diffusion of water through the polymer layer. In analogy with many other authors,[2,30] it is assumed that the degree of crystallinity in the rubbery layer increases with drying time with a characteristic time constant, τ_c. Typical values of τ_c reported are between 10^3 and 10^5 s. The degree of crystallinity remains constant in the glassy state. Consequently, the ratio τ_g/τ_c, where τ_g is the drying time required to reach the transition from rubber to glass, is a measure of the final degree of crystallinity of the layer. The time τ_g and the total drying time, $\tau_0 = H_0(1 - \phi_0)/E$, are simply related by

$$\tau_g = \frac{\phi_g - \phi_0}{1 - \phi_0}\tau_0 \tag{8}$$

Following from the foregoing analysis, we expect that layers characterized by the dimensionless time

$$\tau_g^* = \frac{\tau_g}{\tau_c} \ll 1 \tag{9}$$

will dry rapidly and not exhibit significant crystalline regions whether or not they dry uniformly whereas layers characterized by $\tau_g^* \gg 1$ will exhibit a greater degree of crystallinity.

These ideas of degree of crystallinity and of uniformity of drying can be qualitatively expressed in a two-dimensional space with axes *Pe* and τ_g^* as shown in Figure 2. Layers in each of the four quadrants are expected to exhibit different characteristic drying behavior as indicated. In the following Experimental Section we present drying profiles typical of each of three experimentally accessible regions of this space. The fourth quadrant—that of both large *Pe* number and large τ_g^*— is hard to access since fast evaporation and slow drying are generally inconsistent and the *Pe* number cannot be sufficiently increased using the diffusivity and layer thickness alone.

3. Experimental Section

3.1. Materials. PVOH (MOWIOL grade) with a hydrolysis grade greater than 98.0 mol % and average molecular weight of 61K was obtained from Fluka. Following Ngui and Mallapragada,[2] PVOH solutions in the range 10−30% w/v polymer were prepared by dissolving the powdered polymer in deionized water at 90 °C for 6 h, while solutions in the range 35−45% were kept at 90 °C for a further 18 h. The prepared solutions were cast as layers up to 2 mm thick on 18 × 18 mm^2 glass coverslips which had been previously cleaned in Decon-90 and rinsed in dilute HCl. The MRI experiments were started immediately after casting.

3.2. Methods. One-dimensional composition profiles through layers were obtained using GARField. GARField is a permanent magnet with shaped pole pieces. It is characterized by a static near horizontal magnetic field which is of constant magnitude in the horizontal plane. There is a strong field gradient in the vertical direction. The resonance frequency of the ^{1}H nuclei in a sample in this field is thus a linear function of vertical height. Measurement of this frequency provides the spatial localization. GARField profiling experiments were conducted using standard procedures adopted in our laboratory that have been reported elsewhere.[9] In short, the sample is placed on a sample stage consisting of a small (3 mm diameter) radio-frequency surface sensor which probes through the thickness of a central area of the sample. Mylar tape is adhered to the sensor stage and immediately contacts the lower sample surface, that is, the underside of the glass coverslip. The tape acts as a position and intensity reference for the profiling experiments. The data are recorded in the form of a train of *n* spin echoes generated using a standard quadrature echo sequence of radio-frequency excitation pulses of the form $\alpha_x-\tau-(\alpha_y-\tau-\text{echo}-\tau)_n$, where $\alpha_{x/y}$ is a short radio-frequency pulse of nominal flip angle 90° in the vicinity of the sample and τ is a short delay. In the experiments reported here, measurements were made at a magnetic field strength of 0.7 T and at a gradient strength of ca. 17.5 T/m. Typically, the pulse duration was 0.9 μs and the delay τ was 55 μs. Again, typically $n = 128$ echoes were collected, each echo consisting of 64 or 128 points recorded with a sampling rate of 1.2 or 0.6 μs for thin and thicker layers, respectively. Echoes were Fourier transformed to yield a profile in the gradient direction. In an NMR experiment, the signal intensity in subsequent echoes decays as $\exp(-2i\tau/T_2^{\text{eff}})$, where *i* is the echo number. This

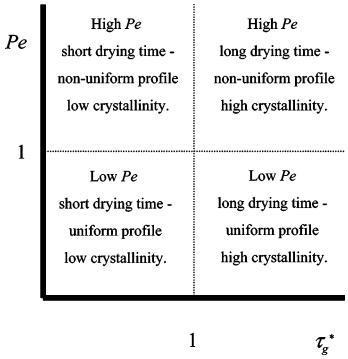

Figure 2. $Pe-\tau_g^*$ space. *Pe* is the (initial) Peclet number of the layer, and τ_g^* is a dimensionless time which characterizes the growth of crystallinity, as described in the text.

provides a powerful contrast mechanism in MRI since the effective spin−spin relaxation time, T_2^{eff}, of the nuclei is an exquisitely sensitive function of molecular motion within the gradient. In the current work the profiles from different echoes were co-added so as to improve the signal-to-noise ratio. The measurement sequence was repeated up to 32 times, depending on the sample evaporation rate, typically at intervals of 5 s and the results were co-added so as to further improve signal-to-noise. The repetition time can itself provide a further contrast mechanism. If it is short compared to the spin−lattice relaxation time of the nuclei, then the signal is attenuated.

For the parameters discussed here, the temporal resolution of measured profiles is as short as 1 min, the nominal spatial resolution is 17 μm, and the field-of-view is 1.1 or 2.2 mm. The useful field-of-view is somewhat less, however, first since the sensitivity of the surface coil decreases markedly with distance from the sensor and second because of the more limited frequency bandwidth of the coil, pulses, and spectrometer. Following our standard practice, profile intensities were normalized by those of a standard elastomer sample of uniform composition. Experiments with $\tau = 95$ μs and a resolution of ca. 9 μm were also recorded but are not shown.

Two-dimensional images of vertical slices across samples were obtained using FLASH[31] MRI. GARField provides only one-dimensional information and at any one height inherently integrates the signal across a small central area of the sample. Therefore, profile artifacts arising from possible curvature of the sample due to meniscus effects are not immediately apparent with GARField. FLASH has the advantage of being multidimensional and more rapid than other 2DFT techniques. However, FLASH yields less quantitative composition data as longer echo times are required (of the order of milliseconds compared to microseconds for GARField). Nonetheless, it differentiates well between liquid and solid. For these reasons, FLASH was used first to confirm conclusions made using GARField and to exclude alternate explanations due to sample curvature or poor sample leveling and second for rewetting experiments where it was necessary to unambiguously differentiate liquid from solid. The FLASH procedure is well-known.[31]

The ^{1}H NMR 2D FLASH images were acquired using a 9 T, 89 mm bore Magnex magnet equipped with a homemade imaging probe-head, specially designed to accommodate planar layers, switched gradients, and a Chemagnetics Infinity spectrometer. A standard gradient-recalled echo sequence was used with an echo time of 0.7 ms and a repetition delay of 7 ms. Excitation was achieved with a 250 μs Gaussian pulse with a flip angle of 5°. The NMR signal was sampled 128 times during the acquisition period, and 64 phase-encoding steps were applied. A sine-bell apodization was applied both in the read direction, corresponding both to the static magnetic field direction and to the vertical direction in the layer, and in the phase direction, corresponding to the horizontal direction. The resultant image field-of-view was 4.8 mm in the vertical direction and 22 mm in the horizontal direction. The spatial resolution (pixel size) was 37 × 344 μm^2. Typically, single images comprising the co-addition of 256 averages with a slice thickness of 2 mm were acquired every few minutes across the center of a drying layer.

The relative humidity in the laboratory was not controlled but tended to be ca. 35%, and the average temperature was 23 °C. In selected experiments the evaporation rate was purposely accelerated or slowed. Faster evaporation rates were achieved by applying a gentle flow of dry air (just detectable on the back of the hand) over the layer surface. Lower water loss rates were obtained by wrapping the conventional MRI probe head in PTFE tape for FLASH and by containing the freshly cast layer at the sealed base of open-top PTFE tubes of variable height for GARField measurements. In the latter case, the water loss rate is limited by the diffusion of water vapor up the tube, away from the sample toward the open end.[32]

To further characterize the materials, the self-diffusivity of the two components of the polymer solutions at different concentrations was measured in equilibrated bulk solution samples. As the self-diffusivities of the two components differ by several orders of magnitude, two different techniques were used.

Spectroscopically resolved pulsed-field-gradient stimulated echo decays[33] were acquired on the 9 T system to measure the self-diffusivity of the water. The echo amplitude decays according to

$$\frac{S}{S_0} = \exp(-\gamma^2 g^2 \delta^2 D_{\text{SW}}(\Delta - \delta/3)) \tag{10}$$

where γ is the magnetogyric ratio, g and δ are the gradient pulse amplitude and duration, respectively, and Δ is the interpulse diffusion time. In the experiments reported, gradient pulses of 2 ms duration and up to 85 G/cm amplitude with diffusion times of 10 and 50 ms were used.

The polymer self-diffusion coefficient was measured with a relaxation-compensated three-pulse stimulated echo sequence in the fringe field[34] of the 9 T system at a static gradient strength of 5800 G/cm and at a resonance frequency of approximately 238 MHz. The first pulse gap, δ, was varied between 60 and 780 μs. The second pulse gap, Δ_1, was 50 ms. The diffusion coefficient is evaluated from the quotient of the intensity of the stimulated, *S*, and primary, *P*, echo signals according to

$$\frac{S}{P} = \exp(-\gamma^2 g^2 \delta^2 D_{\text{SP}} \Delta_1) \tag{11}$$

Last, differential scanning calorimetry (DSC model 2920, TA Instruments) was used to assess the degree of crystallinity of PVOH layers dried under different conditions. DSC measurements were performed at a scanning rate of 10 deg/min from 30 to 255 °C.

4. Results and Discussion

4.1. Diffusion Measurements. Figure 3 shows the echo intensity data from which the water and PVOH self-diffusivities in a 10% equilibrated solution are calculated. The diffusivities are calculated as $(1.48 \pm 0.02) \times 10^{-5}$ and $(3.1 \pm 0.2) \times 10^{-9}$ cm^2 s^{-1}, respectively. These values are in agreement with published data for a deuterated polymer solution at the same concentration and temperature.[35] Data for equilibrated solutions up to 45% w/v polymer yield the diffusivities values for the water and PVOH reported in Figure 4. The self-diffusivity values for water are in agreement with published values for solutions up to 35% w/v polymer.[36] Values for PVOH are comparable to values for other polymers of similar molecular weight and concentration in solution.[37]

A fit to the data for the water in Figure 4 using eq 2 yields D_0 and a values of 2.20×10^{-4} cm^2/s and 2.37,

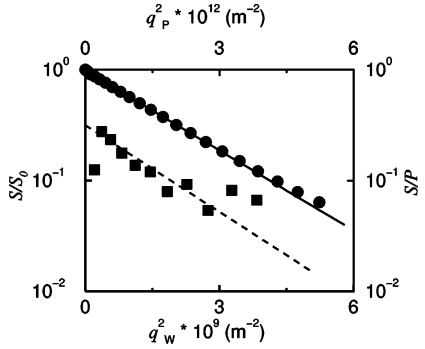

Figure 3. Water proton echo attenuation (circles, left-hand axis), S/S_0, for an equilibrated 10% w/v PVOH aqueous solution as a function of q_W^2, with $q_W = (2\pi)^{-1}\gamma\delta g$. The solid line is a fit to the experimental data according to eq 10, yielding $D_{SW} = 1.48 \times 10^{-5}$ cm^2 s^{-1}. The echo intensity ratio S/P (squares, right-hand axis) for PVOH in the same solution as a function of q_P^2 with $q_P = (2\pi)^{-1}\gamma\delta g$. The dashed line is a fit to the experimental data using eq 11 and excluding the first point which is affected by the water signal. The fit yields $D_{SP} = 3.1 \times 10^{-9}$ cm^2 s^{-1}.

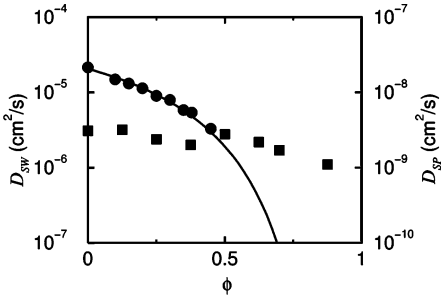

Figure 4. Concentration dependence of the water (circles) and polymer (squares, right-hand axis) self-diffusion coefficient, D_{SW} and D_{SP}, respectively, for the system PVOH−water as a function of the polymer volume fraction ϕ. The solid line is the associated fit to the experimental data for D_{SW} according to eq 2, with $D_0 = 2.20 \times 10^{-4}$ cm^2/s and $a = 2.37$.

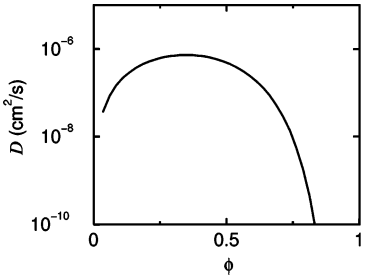

Figure 5. Concentration dependence of the mutual diffusion coefficient, D, for the system PVOH−water as a function of the polymer volume fraction, ϕ, according to eq 5.

respectively. Figure 5 shows a plot of the mutual diffusion coefficient, D, calculated according to eqs 2 and 5 using these fit values and $\chi = 0.49$. The plot in Figure 5 exhibits the broad maximum and strong concentration dependence at high ϕ previously discussed.

4.2. Drying Measurements. We report measurements for the drying of four exemplar layers of PVOH solution, A, B, C, and D. The initial parameters describing the four layers are summarized in Table 1. They are chosen so as to span a broad range of initial Peclet numbers and drying times. The key differences between the layers are suggested by where they sit in the $Pe-\tau_g$* space (Figure 2).

Layer A has a low initial polymer fraction, 10%, a large initial thickness, 1140 μm, and a low initial evaporation rate, $E = 3.0 \times 10^{-7}$ cm/s (see below), to give an initial Peclet number of 0.18 and a value of the dimensionless time parameter for crystals to form of τ_g* = 5.8 assuming $\tau_c = 5 \times 10^4$ s.[3,30] Thus, layer A is typical of the lower right quadrant in Figure 2. Exemplar drying profiles are shown in Figure 6a. For clarity of the figure, MR profiles recorded at 12 h intervals are shown. However, these represent only a small fraction of the total data recorded. As in all the profiles presented here, the profile intensities reflect the mobile and semimobile ^{1}H density. However, with increasing polymer fraction the nuclear spin−lattice relaxation time and water self-diffusivity both decrease. This causes a slight increase for the experimental parameters chosen in the profile intensity in middle profiles before the intensity drops down in the late stages of drying due to the greatly reduced water content. The interface between the polymer solution and the air is on the right;

Table 1. Characteristics of the Drying Layers[a]

layer	initial PVOH concn, % (w/v)	initial layer thickness, H (μm)	initial evaporation rate, E (cm^2/s)	initial Peclet no., Pe	τ_g*
A	10	1140	3.0×10^{-7}	0.18	5.8
B	25	1185	6.4×10^{-6}	1.15	0.25
C	49	1280	5.9×10^{-6}	1.46	0.17
D	10	300	1.5×10^{-6}	0.24	0.32

[a] The Peclet number, Pe, is calculated from the initial parameters. The uncertainty on the layer thickness is ± 10 μm. τ_g* is a dimensionless time, which characterizes the growth of crystallinity of the layer.

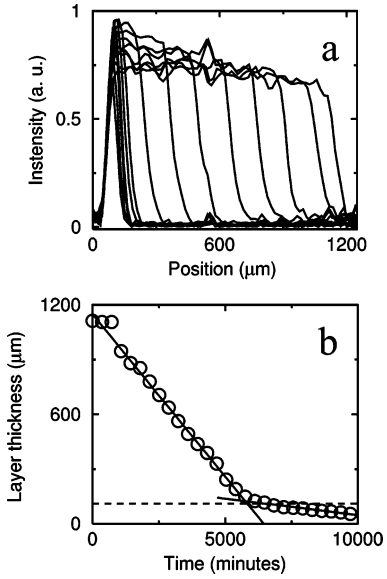

Figure 6. (a**)** GARField MR profiles, after normalization by an elastomer standard, of layer A drying under controlled conditions. As in all profiles shown, the air surface is on the right and the substrate interface is on the left. The initial PVOH concentration is 10%, and H_0 is 1140 μm. Profiles are shown every 12 h. The repetition time is 10 s, and the number of averages was increased in the late stages of the experiment, hence the higher signal-to-noise ratio. The signal intensity still present after 6.5 days is due to residual water in the layer. **(**b**)** The thickness of layer A as a function of time estimated from the width of the profiles shown in (a). The two solid lines are linear fits to the experimental data from 0 to 5700 min ($E = 3.0 \times 10^{-7}$ cm/s) and from 5700 min until the end of the drying process ($E = 3.0 \times 10^{-8}$ cm/s), respectively. The dashed line is the predicted final thickness of the layer calculated from the initial experimental thickness and the initial concentration of the solution.

the interface with the glass substrate is on the left. The profile intensities are normalized to an elastomer standard to remove the effect of decreasing detector sensitivity with distance from the coil. With time and as the evaporation proceeds, the profile width decreases from the right. The profile width is shown in Figure 6b as a function of time.

Two observations are made. First, the concentration profiles are characterized by a generally rectangular shape indicating a broadly uniform composition across the layer depth throughout the drying period. Second, the drying period divides naturally into two stages. In the first stage, lasting ca. 3.5 days, the profile width decreases uniformly with time, yielding the evaporation rate of 3.0×10^{-7} cm/s. In the second stage, the drying slows dramatically ($E = 3.0 \times 10^{-8}$ cm/s), and the apparent layer thickness decreases substantially below that expected on the basis of the initial 10% polymer fraction (dotted horizontal line in Figure 6b). After 6.5 days there is still some residual mobile ^{1}H (water) in the layer. These results can be explained by the formation of a glassy skin layer after 3.5 days and the trapping of water in the lowest layers beneath the skin. The glassy skin itself has insufficient mobile ^{1}H to be visualized, and hence the apparent profile thickness is less than the theoretical minimum layer thickness. We note that the evaporation slows when the water fraction is a little above 10%, close to the predicted value of 13% for the glass transition. The dramatic slowdown in evaporation compared to other layers yet to be discussed suggests that the glassy skin is particularly impermeable from which we infer a relatively high crystalline fraction. These observations are in agreement with the work of Ngui and Mallapragada.[3] These authors observed a change in gradient in the weight of drying PVOH solution layers with time and attributed this change in gradient to the transition of the polymer from the rubbery state to the glassy state by thermogravimetric analysis and dynamic mechanical analysis.

The behavior of layer A is contrasted to that of layer B. Layer B has a higher initial polymer fraction, 25%, a comparable initial thickness, 1185 μm, and a substantially higher initial evaporation rate, $E = 6.4 \times 10^{-6}$ cm/s, to give a larger initial Peclet number of 1.15 and a much smaller $\tau_g^* = 0.25$. This places the layer nearer the upper left quadrant of the $Pe-\tau_g^*$ space. Exemplar profiles are shown at 28 min intervals in Figure 7a. Again the profiles recede from the right as evaporation proceeds. However, unlike the profiles in Figure 6, the profile intensity is not uniform across the profile width throughout the majority of the drying time. This suggests that the water concentration is not uniform across the layer depth; rather, it is less near the air interface. The overall water fraction can be gauged from the layer thickness which is shown in Figure 7b. This plot shows that the evaporation rate is initially uniform but that it slows down over a broad transition region between 150 and 250 min to 1.1×10^{-6} cm/s. The start of the transition zone is taken as 150 min, at which time the overall polymer fraction in the layer is ca. 60%. This is much greater than ϕ_g. However, the profiles make clear that the polymer concentration at the air interface is substantially less than 60%. The suggestion is that a "skin" layer is forming. However, as the drying does not slow so dramatically as in layer A, the inference is that the skin is not so impermeable as for layer A. Indeed,

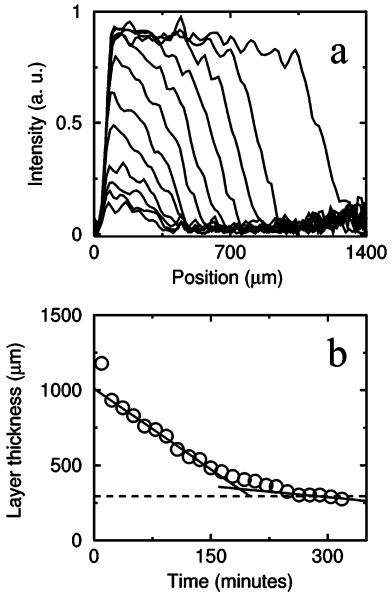

Figure 7. (a) GARField MR profiles, after normalization by an elastomer standard, of layer B drying under a gentle flow of dry air. The initial PVOH concentration is 25% and H_0 is 1185 μm. Profiles are shown every ≈28 min. (b) Thickness of layer B as a function of time estimated from the width of the profiles shown in (a). The two solid lines are linear fits to the experimental data from 0 to 150 min ($E = 6.4 \times 10^{-6}$ cm/s) and from 270 min until the end of the drying process ($E = 1.3 \times 10^{-6}$ cm/s), respectively. The dashed line is the predicted final thickness of the layer calculated from the initial experimental thickness and the initial concentration of the solution.

one can ask whether a "skin" is really formed or whether the experiment merely provides evidence of nonuniform drying.

Layer C is similar to layer B except that the Peclet number is even larger, $Pe = 1.46$, and the dimensionless time τ_g^* slightly less, 0.17, pushing the layer further into the upper left quadrant. In this layer, the initial polymer fraction is 49%. This concentration is achieved by very slow evaporation of the 25% solution. Exemplar profiles and the time dependence of the layer thickness are shown in parts a and b of Figure 8, respectively. The trend to nonuniform drying and weak skin formation observed in layer B are seen yet more strongly here.

The upper left and lower right quadrants of the $Pe-\tau_g^*$ space in Figure 2 are relatively easy to explore experimentally and reveal the contrasting behavior already discussed. The lower left quadrant is more difficult to access, and we have been unable to produce a layer in the upper right quadrant. Layer D is in the lower left quadrant. This layer is much thinner, $H_0 = 300$ μm, than any of A, B, or C. The evaporation rate is intermediate at $E = 1.46 \times 10^{-6}$ cm/s. The Peclet number is $Pe = 0.24$ and $\tau_g^* = 0.32$, much less than layer A. The profiles in Figure 9a and the time dependence of the layer thickness shown in Figure 9b reveal the expected behavior. Consistent with a low Peclet number, the layer concentration profiles are essentially rectangular, indicating uniform drying. Equally consistent with a low τ_g^*, there is no evidence of a crystalline skin forming. Rather, the thickness decreases linearly to that expected of the dry layer without a transition to a period of much slower evaporation.

4.3. Rewetting Measurements. Further evidence of differentiation between layers of high Peclet number dried quickly and layers of low Peclet number dried more slowly is afforded by experiments in which a fresh

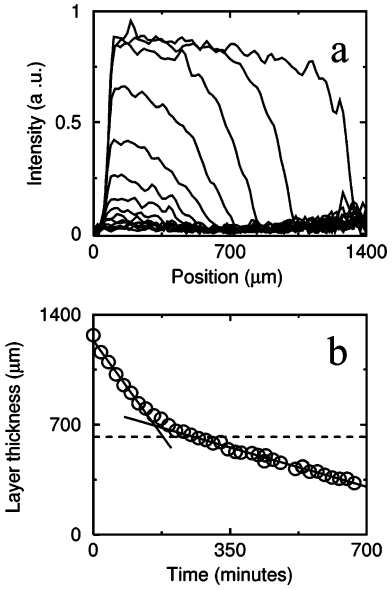

Figure 8. (a) GARField MR profiles, after normalization by an elastomer standard, of layer C, with an initial PVOH concentration of 49%, drying under a gentle flow of dry air. H_0 is 1280 μm. Profiles are shown every ≈77 min. The layer was prepared by slow drying of 25% solution. (b) Thickness of layer C as a function of time estimated from the width of the profiles shown in (a). The two solid lines are linear fits to the experimental data from 0 to 130 min ($E = 5.9 \times 10^{-6}$ cm/s) and from 220 min until the end of the drying process ($E = 1.3 \times 10^{-6}$ cm/s), respectively. The dashed line is the predicted final thickness of the layer calculated from the initial experimental thickness and the initial concentration of the solution.

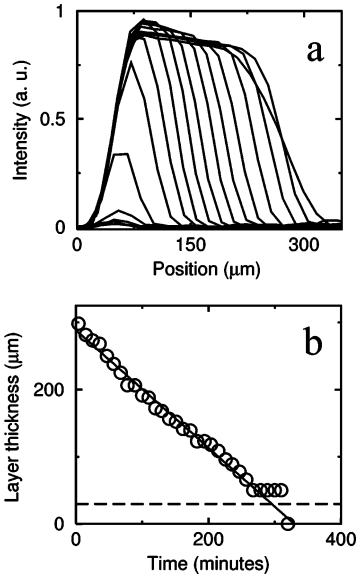

Figure 9. (a) GARField MR profiles, after normalization by an elastomer standard, of layer D drying under controlled conditions. The initial PVOH concentration is 10% and H is 300 μm. Profiles are shown every 21.3 min. (b) Thickness of layer D as a function of time estimated from the width of the profiles shown in (a). The solid line is a linear fit to the data with $E = 1.5 \times 10^{-6}$ cm/s.

layer of solution is applied above the dried layer. As an example, Figure 10a shows five profiles extracted from FLASH MRI images recorded for a wet on dry layer, the latter typical of the upper left quadrant in Figure 2. The initial solution was 25% PVOH. The layer was allowed to dry rapidly over 7 h until the water fraction was below 1%, at which point the layer was judged to

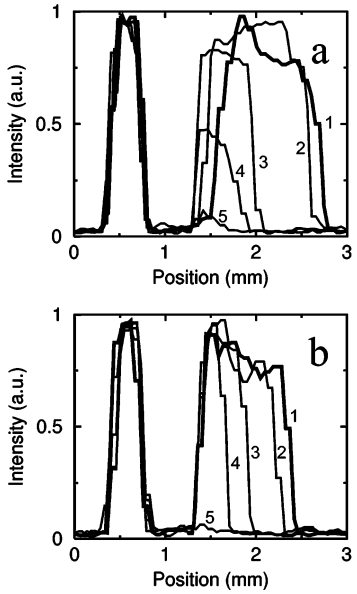

Figure 10. (a) Central profiles extracted from ^{1}H NMR FLASH images for a 25% PVOH layer dried under a gentle flow of air for 7 h until the water fraction was below 1% with a second wet layer added above. There is no signal from the dried layer. The peak to the left is a reference oil layer and that to the right the wet layer. Profiles are shown 14 min (thick line, profile 1), 2.1, 5.9, 7.2, and 21 (profile 5) hours after the wet layer was added. The wet layer ingresses the dry layer from about 1.5 to 1.3 mm on the scale. (b) Central profiles extracted from images for a 10% PVOH layer dried slowly for 7 days until the water fraction was below 1% with a second wet layer added above. Profiles are shown 10 min (thick line, profile 1), 2.1, 5.7, 7.2, and 23.3 h after the wet layer was added. The wet layer does not ingress the dry layer.

be ca. 235 μm thick based on gravimentric and area analysis. At this point, further 10% solution was added above the layer and the sample placed in the magnet for imaging. The first profile in the figure was recorded as soon as practically possible (14 min) after the wet layer was applied. It shows the wet layer to the right immediately above the (not visualized) dry layer. Below this are glass coverslips which separate the PVOH layers from a layer of oil which acts as a position reference marker. The oil is clearly seen to the left of the figure. The position scale has been accurately calibrated using images of multiple oil−coverslip sandwiches. The following profiles in the figure show how the wet layer subsequently invades the dry layer and also itself dries. After 6 h, the wet layer has diffused the full thickness of the dry layer.

This is to be contrasted with the results for a wet on dry layer with the latter typical of the lower right quadrant of Figure 2. In this case, the dry layer was cast from 10% solution and is estimated to be 100 μm thick. The layer was dried slowly, over 8 days. The profiles shown in Figure 10b were recorded at times comparable to those in Figure 10a. In this case the wet layer does not invade the dry layer before it dries. Our interpretation of this key difference is entirely consistent with our previous analysis. We suggest that the lower dry layer in Figure 10b is likely more crystalline than that in Figure 10a. The crystalline layer presents a much less permeable barrier to the wet solution placed on top.

4.4. DSC Measurements. The DSC thermographs of the dried layers exhibit a sharp peak at about 225 °C. This peak is characteristic of the melting of the

PVOH crystallites, and the area under the melting curve is proportional to the heat required for the melting process. The heat of melting for a 100% crystalline PVOH sample is known from the literature to be 138.6 J/g.[38] Typical values reported for dried PVOH layers in the literature range up to 50%. The higher crystallinity is usually found after a high-temperature annealing.[39] It is found that the degree of crystallinity for the dried layer A is 49.5%, for layer B it is 36.4%, and for layer C it is 33.6%. No measurement was made for layer D.

In agreement with the suggestions of the MRI data and the calculated τ_g*, the degree of crystallinity of the dried layers depends on the drying experimental conditions: drying the PVOH solution in slow controlled conditions causes an ordering of the polymer, leading to an increase of the degree of crystallinity.

5. Conclusions

Magnetic resonance imaging has afforded considerable new insight into the drying of polymer layers. It has enabled direct visualization for the first time of the water concentration profile. Profiles have been recorded for initial Peclet numbers and drying times, each spanning an order of magnitude. It has been shown that the drying characteristics can be broadly estimated from the position of the layer in a two-dimensional parameter space defined by the Peclet number and a dimensionless drying time. The results show that the uniformity of composition of the drying layer is a strong function of initial Peclet number. Layers dried sufficiently slowly show a uniform composition whereas layers dried more quickly do not. In addition, it is inferred that the top surface of the drying layer develops into a crystalline skin for layers dried slowly in comparison to the characteristic time for the glass−crystalline transition. These conclusions are supported by rewetting and differential scanning calorimetry experiments.

Acknowledgment. E.C. thanks Unilever Research for financial support.

References and Notes

(1) Romdhane, I. H.; Price, P. E.; Miller, C. A.; Benson, P. T.; Wang, S. *Ind. Eng. Chem. Res.* **2001**, *40*, 3065−3075.
(2) Ngui, M. O.; Mallapragada, S. K. *J. Polym. Sci., Polym. Phys.* **1998**, *36*, 2771−2780.
(3) Ngui, M. O.; Mallapragada, S. K. *J. Polym. Sci., Polym. Phys.* **1999**, *72*, 1913−1920.
(4) Ngui, M. O.; Mallapragada, S. K. *Polymer* **1999**, *40*, 5393−5400.
(5) Vinjamur, M.; Cairncross, R. A, *J. Appl. Polym. Sci.* **2003**, *87*, 477−486.
(6) Yoshida, M.; Miyashita, H. *Chem. Eng. J.* **2002**, *86*, 193−198.
(7) Narasimhan, B.; Snaar, J. E. M.; Bowtell, R. W.; Morgan, S.; Melia, C. D.; Peppas, N. A. *Macromolecules* **1999**, *32*, 704−710.
(8) Glover, P. M.; Aptaker, P. S.; Bowler, J. R.; Ciampi, E.; McDonald, P. J. *J. Magn. Reson.* **1999**, *139*, 90−97.
(9) Wallin, M.; Glover, P. M.; Hellgren, A. C.; Keddie, J. L.; McDonald, P. J. *Macromolecules* **2000**, *33*, 8443−8452.
(10) Gorce, J.-P.; Bovey, D.; McDonald, P. J.; Palasz, P.; Taylor, D.; Keddie, J. L. *Eur. Phys. J. E* **2002**, *8*, 421−429.
(11) Mallégol, J.; Barry, A. M.; Ciampi, E.; Glover, P. M.; McDonald, P. J.; Keddie, J. L.; Wallin, M.; Motiejauskaite, A.; Weissenborn, P. K. *J. Coat. Technol.* **2002**, *74*, 113−124.
(12) Bennett, G.; Berglind, H.; Gorce, J.-P.; Keddie, J. L.; McDonald, P. J. *Magn. Reson. Imaging* **2003**, *21*, 235−241.
(13) Callaghan, P. T. *Principles of Nuclear Magnetic Resonance Microscopy*; Oxford University Press: New York, 1995.
(14) Kimmich, R. *NMR, Tomography, Diffusometry, Relaxometry*; Springer-Verlag: Berlin, 1997.
(15) Routh, A. F.; Russell, W. B. *Langmuir* **1999**, *15*, 7762−7773.
(16) de Gennes, P. G. *Eur. Phys. J. E* **2002**, *7*, 31−34.
(17) Vrentas, J. S.; Ventras, C. M. *Eur. Polym. J.* **1998**, *34*, 797−803.
(18) Zhong, C.; Qu, Y.; He, J. *J. Chem. Eng. Jpn.* **2001**, *34*, 1493−1498.
(19) Liu, Q.-L.; Gao, H.-Q. *J. Membr. Sci.* **2003**, *214*, 131−142.
(20) Vrentas, J. S.; Duda, J. L. *J. Polym. Sci., Polym. Phys. Ed.* **1977**, *15*, 403−416.
(21) Vrentas, J. S.; Duda, J. L. *AIChE J.* **1979**, *25*, 1−24.
(22) Duda, J. L.; Vrentas, J. S.; Ju, S. T.; Liu, H. T. *AIChE J.* **1982**, *28*, 279−285.
(23) Vrentas, J. S.; Ventras, C. M. *Macromolecules* **1993**, *26*, 6129−6131.
(24) Zielinski, J. M.; Hanley, B. F. *AIChE J.* **1999**, *45*, 1−12.
(25) Peppas, N. A.; Wu, J. C.; von Meerwall, E. D. *Macromolecules* **1994**, *27*, 5626−5638.
(26) Alsoy, S.; Duda, J. L. *AIChE J.* **1999**, *45*, 896−905.
(27) Sperling, L. H. *Introduction to Physical Polymer Science*, 2nd ed.; Wiley: New York, 1992; p 75.
(28) In *Polymer Handbook*, 4th ed.; Brandrup, J., Immergut, E. H., Grulke, E. A., Eds.; Wiley: New York, 1999.
(29) Rasmussen, D. H.; MacKenzie, A. P. *J. Phys. Chem.* **1971**, *75*, 967−973.
(30) Mallapragada, S. K.; Peppas, N. A. *AIChE J.* **1997**, *43*, 870−876.
(31) Haase, A.; Frahm, J.; Matthaei, D.; Hanicke, W.; Merboldt, K. D. *J. Magn. Reson.* **1986**, *67*, 256−258.
(32) Ciampi, E.; Goerke, U.; Keddie, J. L.; McDonald, P. J. *Langmuir* **2000**, *16*, 1057−1065.
(33) Tanner, J. E. *J. Chem. Phys.* **1970**, *52*, 2523−2526.
(34) Kimmich, R.; Fisher, E. *J. Magn. Reson. A* **1994**, *106*, 229−235.
(35) Shapiro, Y. E. *Colloids Surf. A: Physicochem. Eng. Aspects* **2000**, *164*, 71−83.
(36) Petit, J.-M.; Zhu, X. X.; Macdonald, P. M. *Macromolecules* **1996**, *29*, 70−76.
(37) Chekal, B. P.; Torkelson, J. M. *Macromolecules* **2002**, *35*, 8126−8138.
(38) Mallapragada, S. K.; Peppas, N. A. *J. Polym. Sci., Part B: Polym. Phys.* **1996**, *34*, 1339−1346.
(39) Peppas, N. A.; Merrill, E. W. *J. Polym. Sci., Polym. Chem.* **1976**, *14*, 441−457.

MA034951J